Role of different parts of the nucleon-nucleon potential on fragment production in asymmetric collisions and their rapidity dependence

Manpreet Kaur,[1] Mandeep Kaur,[2] and Varinderjit Kaur[3,*]
[1]*Department of Physics, Sri Guru Granth Sahib World University, Fatehgarh Sahib 140406, India*
[2]*School of Physics and Materials Science, Thapar University, Patiala 147004, Punjab, India*
[3]*Department of Physics, Mata Gujri College, Fatehgarh Sahib 140406, India*
(Received 7 May 2017; published 30 August 2017)

The role of different parts of the nucleon-nucleon (NN) interaction potential on the production of light- and intermediate-mass fragments in different mass asymmetric reactions ^{120}Sn + ^{120}Sn ($\eta = 0$), ^{82}Kr + ^{158}Gd ($\eta = 0.3$), ^{56}Fe + ^{184}W ($\eta = 0.5$), and ^{35}Cl + ^{205}Tl ($\eta = 0.7$) (with $A_{\text{total}} = 240$ units) within different rapidity domains has been investigated using the isospin-dependent quantum molecular-dynamics model. The results indicate that the multiplicity of different fragments changes with the gradual addition of different parts of the NN interaction potential. The comparison between calculations and experimental data for the ^{120}Sn + ^{120}Sn reaction reveals that both momentum dependent interactions (MDIs) and symmetry potential are indispensable to explain the charge distribution. The MDI plays a dominant role while the symmetry potential has minor influence on the fragment production, but both together lead to an increase in the multiplicity of light- and intermediate-mass fragments and hence show their significance in the fragment production at intermediate energies.

DOI: 10.1103/PhysRevC.96.024626

I. INTRODUCTION

Innovations in the field of heavy-ion reaction technology allow one to use a variety of projectile and target combinations, which help one to understand nuclear reaction dynamics in different energy domains. The energy of the projectile in a nuclear reaction governs the reaction dynamics. In the low-energy regime ($\sim E \leqslant 10$ MeV/nucleon), the mean nuclear field acting between the two nuclei dominates and nucleon-nucleon collisions are insignificant due to lack of available phase space. The main interest of low-energy heavy-ion experiments is to study fusion dynamics, nuclear structure, synthesis of superheavy elements, exotic nuclei, behavior of nuclei under different conditions, etc. [1–4]. The dominant mode of decay is the binary fragmentation at low energies. With an increase in energy, at the intermediate-energy regime (10 MeV/nucleon $< E <$ 2 GeV/nucleon), both the mean-field and nucleon-nucleon collisions play their role. The different phenomena in this energy region are multifragmentation, nuclear flow, fragment flow, nuclear stopping, etc. [5–10].

During a nuclear reaction, the interaction between projectile and target nucleons takes place and the outcome of a reaction depends strongly on the interaction potential, which is the imperative factor in deciding the fate of a nuclear reaction. Therefore, knowledge of the nucleon-nucleon (NN) interaction potential is the fundamental theoretical tool in the analysis of heavy-ion reactions (HIRs). It is a key ingredient for constructing the nuclear equation of state. Many attempts have been made in the literature to study the mechanism behind the HIRs by using the NN interaction potential [11–13]. The general trend of using the NN interaction potential in the simulation of HIRs is to parametrize the same as a function of density (as it is done for the Skyrme interaction) [13]. While parametrizing the potential, one begins with the fundamental interaction, i.e., Skyrme interaction, and then adds other components of potential such as the Yukawa potential, Coulomb potential, momentum dependent interaction (MDI), and symmetry potential. Thus the total interaction potential is the sum of Skyrme, Yukawa, Coulomb, MDI, and symmetry potentials.

Skyrme and Yukawa are the two basic potentials which correspond to the number of nucleons present in the core of the nucleus and on the surface of the nucleus, respectively, and hence represent the volume and surface terms in the semiempirical liquid drop mass formula. In past decades, extensive attempts have been made using various parametrizations of the density dependent Skyrme potential to understand heavy-ion collision dynamics at low energies [14,15]. Skyrme interactions have also been used extensively in the literature to study such effects at intermediate energies [16–18]. Also, the Coulomb potential is an important asymmetry term which brings isospin effect at intermediate-energy HIRs. The effect of the Coulomb potential is greater in the case of heavier systems and it increases with colliding geometry since it will push a greater number of nucleons in the transverse direction away from the participant zone. The Coulomb potential is found to affect fragment production at intermediate energies [19–21]. The Coulomb potential is also found to affect the balance energy drastically [22].

In addition, the momentum dependent potential also plays a crucial role in the dynamics of HIRs. The relative momentum between interacting protons and neutrons is small as long as the projectile and target nuclei do not overlap and hence the MDI does not play a role at that time. As soon as the projectile and target nuclei begin to overlap, the nucleons of very large relative momentum come close to each other. Due to this large relative momenta, the projectile nucleons feel a very strong repulsion from the target nucleons and leave the participant/overlap zone by gaining transverse momentum and

*drvarinderjit@gmail.com

hence the role of MDI comes into the picture. The studies show that momentum dependence of the NN potential has significant influence on collective flow [13,23,24], particle production [25], and fragment production [26]. The study of the effect of MDI, within the Vlasov-Uehling-Uhlenbeck approach, on the energy of vanishing flow (EVF) reveals that MDI reduces the EVF in lighter systems in comparison to heavier ones [27].

The symmetry potential, an important part of the NN potential, helps one to understand astrophysical systems, e.g., supernova explosions, neutron stars, etc. It accounts for the larger neutron content in isospin asymmetric systems. It can be defined as the difference of energy per nucleon between pure neutron matter and symmetric nuclear matter, i.e., the energy required to convert all the protons in symmetric nuclear matter to all the neutrons at a fixed density [28]. The symmetry energy tends to play a significant role during the overlapping and dissociation stage. The density dependence of symmetry energy affects nuclear dynamics at the time when the density of the system is above the normal nuclear matter density. The large variation of density during the nuclear reaction leads to significant variation in symmetry energy strength and hence a more accurate picture of density dependent symmetry energy can be obtained. From various theoretical models, the value of symmetry energy is found to be around 30–32 MeV at normal nuclear matter density [29], the same as determined from the semiempirical liquid drop mass formula. The symmetry potential has also been found to affect transverse flow [30]. The density dependence of symmetry energy has been explored at subsaturation densities by investigating its effect on isospin diffusion in peripheral "isospin-asymmetric" collisions of $^{112}\mathrm{Sn} + ^{124}\mathrm{Sn}$ at $E = 50$ MeV/nucleon and the pre-equilibrium neutron to proton transverse emission ratio in $^{112,124}\mathrm{Sn} + ^{112,124}\mathrm{Sn}$ reactions [31,32]. Theoretical calculations of the above observables, within improved quantum molecular-dynamical theory, present consistent constraints on density dependence of symmetry energy [33]. The momentum dependence of the nucleon potential and the symmetry energy considerably affects the isospin diffusion. The momentum dependence of the isoscalar nuclear potential and the symmetry potential affects two-nucleon correlation functions and light cluster production. Also, the impact of isospin and the momentum dependent nuclear potential on the thermal properties of hot asymmetric nuclear matter formed in HIRs has been studied [34–36]. The role of different parts of the NN potential on the energy of vanishing flow has been investigated [37], but it needs to be further explored how these different parts of the NN interaction potential affect fragment production at intermediate energies by considering the effect of mass asymmetry of the reaction.

In HIRs, the phase-space configuration of the clusters produced is characterized by the degree of chaoticity produced in the reaction after the freeze-out density. Due to an interplay between compression and expansion, the excited nuclei disintegrate into a number of light-, intermediate-, and heavy-mass clusters. The yield of these highly excited clusters depends on the contribution of various parts of the NN interaction potential. In addition to input parameters/ingredients of a reaction, i.e., incident beam energy, masses of colliding nuclei, impact parameter, etc., the mass asymmetry [$\eta = (A_T\text{-}A_P)/(A_T + A_P)$] of the reaction plays a remarkable role in the reaction dynamics. In the symmetric reaction ($\eta = 0$), the excitation energy is available in the form of compressional energy in contrast to the asymmetric reaction ($\eta \neq 0$) where the excitation energy is stored in the system mostly in the form of thermal energy due to reduced compression. We can also say that compression is certainly reduced in mass asymmetric reactions as compared to mass symmetric reactions. Moreover, some amount of available energy (even a small portion) always goes away in the compression/expansion degree of freedom. The aim of multifragmentation studies is to relate experimental observations to the properties of the nuclear matter phase diagram. The onset of clusterization affects significantly the kinematical properties of clusters, which can provide useful information about the equation of state of hot and dense nuclear matter and other phenomena at intermediate energies.

The production of fragments in the different rapidity domains measured after the collision of heavy ions is one of the interesting observations to study the HIRs. The rapidity distribution is an important parameter to explore the contribution of the participant and spectator matter in HIRs at intermediate energies. Two methods have been reported in the literature to differentiate between participant and spectator matter. In one of the methods, a nucleon is considered to be originating from the participant if it has undergone at least single collision. A nucleon which has not undergone even a single collision is treated as a spectator nucleon. Alternatively, one can define participant spectator matter in terms of rapidity distribution $|\frac{Y_{\mathrm{c.m.}}}{Y_{\mathrm{beam}}}|$, which is defined as

$$Y(i) = \frac{1}{2} \ln \frac{E(i) + p_z(i)}{E(i) - p_z(i)} \tag{1}$$

where $E(i)$ and $p_z(i)$ are the total energy and longitudinal momentum of the ith particle, respectively. Here, the different cuts in rapidity distribution can be imposed to differentiate between the participant and spectator matter [38].

In the present paper, to explore the contribution of different parts of the NN interaction potential towards fragment production in different rapidity domains, the complete range of rapidity distribution is divided into two different regions, namely, the participant rapidity (PR) region and quasiparticipant rapidity (QPR) region. The PR region is defined as $|\frac{Y_{\mathrm{c.m.}}}{Y_{\mathrm{beam}}}| \leqslant 0.5$ and the QPR region is defined as $|\frac{Y_{\mathrm{c.m.}}}{Y_{\mathrm{beam}}}| > 0.5$. It is important to mention here that the correlation between the shape of the rapidity distribution of light charged particles (LCPs) and different fragmentation modes in the semiperipheral collisions of symmetric reactions has been studied recently [39]. The study shows that a greater number of LCPs at the midrapidity region emerge from binary and ternary breakup modes in comparison to the multifragment breakup mode. A lot of findings are present in the literature on the fragmentation of light- as well as intermediate-mass fragments (IMFs) [40–42], but the contribution of different parts of the NN interaction potential towards the aforesaid observables within different rapidity regions with the varying mass asymmetry needs further investigation. The role of different parts of the NN potential on the energy of vanishing

flow has been explored [37], yet the role of different parts of the NN potential on multifragmentation needs to be studied. Therefore, we intend to investigate the dependence of fragment production (LCPs, IMFs) and reaction dynamics on different parts of the NN interaction potential in PR as well as QPR regions in mass asymmetric collisions with $A_{\rm total} = 240$ units. In Sec. II a brief methodology of the isospin-dependent quantum molecular-dynamics (IQMD) model is presented. Results are discussed in Sec. III leading to the conclusions in Sec. IV.

II. ISOSPIN-DEPENDENT QUANTUM MOLECULAR DYNAMICS MODEL

The present paper is carried out within the IQMD approach [43,44], a modernized version of the QMD model developed by Aichelin and coworkers [25,45–47]. The IQMD model has been used successfully to explain various phenomena such as fragmentation [5,6], collective flow [7,8], elliptical flow [9], and nuclear stopping [10] successfully. The isospin degree of freedom enters into the calculations via symmetry potential, cross sections, and Coulomb interactions. In the IQMD model, the nucleons of target and projectile interact via two- and three-body Skyrme forces, Yukawa potential, and Coulomb interactions. In addition to the use of explicit charge states of all baryons and mesons, a symmetry potential between protons and neutrons corresponding to the Bethe-Weizsacker mass formula has been included. In this model, baryons are represented by wave packets:

$$f_i(\vec{r},\vec{p},t) = \frac{1}{(\pi\hbar)^3}\cdot e^{-[\vec{r}-\vec{r}_i(t)]^2/2L}\cdot e^{-[\vec{p}-\vec{p}_i(t)]^2 2L/\hbar^2}. \quad (2)$$

The centroids of these wave packets propagate using classical Hamilton equations of motion:

$$\frac{d\vec{r}_i}{dt} = \frac{d\langle H\rangle}{d\vec{p}_i}; \quad \frac{d\vec{p}_i}{dt} = -\frac{d\langle H\rangle}{d\vec{r}_i} \quad (3)$$

with

$$\begin{aligned}\langle H\rangle &= \langle T\rangle + \langle V\rangle \\ &= \sum_i \frac{p_i^2}{2m_i} + \sum_i\sum_{j>i}\int f_i(\vec{r},\vec{p},t)V^{ij}(\vec{r}',\vec{r}) \\ &\quad\times f_j(\vec{r}',\vec{p}',t)d\vec{r}d\vec{r}'d\vec{p}d\vec{p}'. \end{aligned} \quad (4)$$

The baryon-baryon potential V^{ij}, in the above relation, reads as

$$\begin{aligned}V^{ij}(\vec{r}'-\vec{r}) &= V^{ij}_{\rm Skyrme} + V^{ij}_{\rm Yukawa} + V^{ij}_{\rm Coul} + V^{ij}_{\rm sym} + V^{ij}_{\rm MDI} \\ &= \left[t_1\delta(\vec{r}'-\vec{r}) + t_2\delta(\vec{r}'-\vec{r})\rho^{\gamma-1}\left(\frac{\vec{r}'+\vec{r}}{2}\right)\right] \\ &\quad + t_3\frac{\exp(-|\vec{r}'-\vec{r}|/\mu)}{(|\vec{r}'-\vec{r}|/\mu)} + \frac{Z_iZ_je^2}{|\vec{r}'-\vec{r}|} \\ &\quad + t_4\frac{1}{\varrho_0}T_3^iT_3^j\delta(\vec{r}'-\vec{r}) \\ &\quad + t_5\ln^2[t_6(\vec{p}'-\vec{p})^2+1]\delta(\vec{r}'-\vec{r}). \end{aligned} \quad (5)$$

Here Z_i and Z_j denote the charges of ith and jth baryons. The parameters μ and $t_1,\ldots,t_6$ are adjusted to the real part of the nucleonic optical potential. In the limit of infinite nuclear matter, the static Skyrme interaction [in Eq. (5)] reduces to the density dependent potential

$$U_{\rm loc} = \alpha(\rho/\rho_0) + \beta(\rho/\rho_0)^2.$$

The above two parameters (α,β) are fixed by the requirement that the average binding energy (at normal nuclear matter density ρ_0) should be -15.76 MeV and the total energy should have a minimum at ρ_0. To understand the role of different compressibilities, the above potential can be generalized to

$$U_{\rm loc} = \alpha(\rho/\rho_0) + \beta(\rho/\rho_0)^\gamma.$$

The momentum dependent interaction is obtained by parametrizing the momentum dependence of the real part of the optical potential. The final form of the potential reads as in Ref. [45]:

$$U_{\rm MDI} = t_4\ln^2[t_5(p_1-p_2)^2+1]\delta(r_1-r_2). \quad (6)$$

A parameterized form of the local plus momentum dependent interaction potential is given by $U = \alpha(\rho/\rho_0) + \beta(\rho/\rho_0)^\gamma + \delta\ln^2[\epsilon(\rho/\rho_0)^{2/3}+1]\,(\rho/\rho_0)^\gamma$.

In the above equation the parameters α, β, and γ must be readjusted in the presence of momentum dependent interactions so as to reproduce the ground-state properties of nuclear matter. The set of parameters corresponding to soft (S), hard (H), and their momentum dependent versions SM and HM, respectively, can be found in Refs. [25,45].

The phase space generated with the IQMD model is stored at different time steps and analyzed using the minimum spanning tree (MST) clusterization algorithm. This approach has been quite successful in explaining certain fragmentation observables such as IMF multiplicities, charge distribution of emitted particles, etc. [25]. In the MST method, two nucleons are allowed to share the same fragment if their centroids are closer than a distance $r_{\rm min}$, $|r_i - r_j| \leqslant r_{\rm min}$, where r_i and r_j are the spatial positions of both nucleons, where $r_{\rm min}$ is 4 fm. The clusterization algorithm is applied at 200 fm/c.

III. RESULTS AND DISCUSSION

In the present paper, several thousand events have been simulated for the central collisions of the reactions ^{120}Sn + ^{120}Sn ($\eta = 0$), ^{82}Kr + ^{158}Gd ($\eta = 0.3$), ^{56}Fe + ^{184}W ($\eta = 0.5$), and ^{35}Cl + ^{205}Tl ($\eta = 0.7$) at incident energies between 50 and 200 MeV/nucleon. In order to study the role of mass asymmetry of the reaction, the reactions are chosen in such a way that the mass asymmetry of the reactions varies between 0 and 0.7 while the total mass remains constant, i.e., $A_{\rm total} = 240$ units. It has been stated in Refs. [48,49] that the results obtained with $\sigma_{nn}^{\rm free}$ deviate from the experimental data by 25%. So, a reduced cross section $\sigma_{\rm red} = 0.8\sigma_{nn}^{\rm free}$ is used in the present paper. The details about the elastic and inelastic cross sections for proton-proton and proton-neutron collisions can be found in Refs. [43,44]. To study the contribution of different parts of the NN interaction potential in different observables, one may begin with the basic potential and then resimulate the reaction each time by gradual

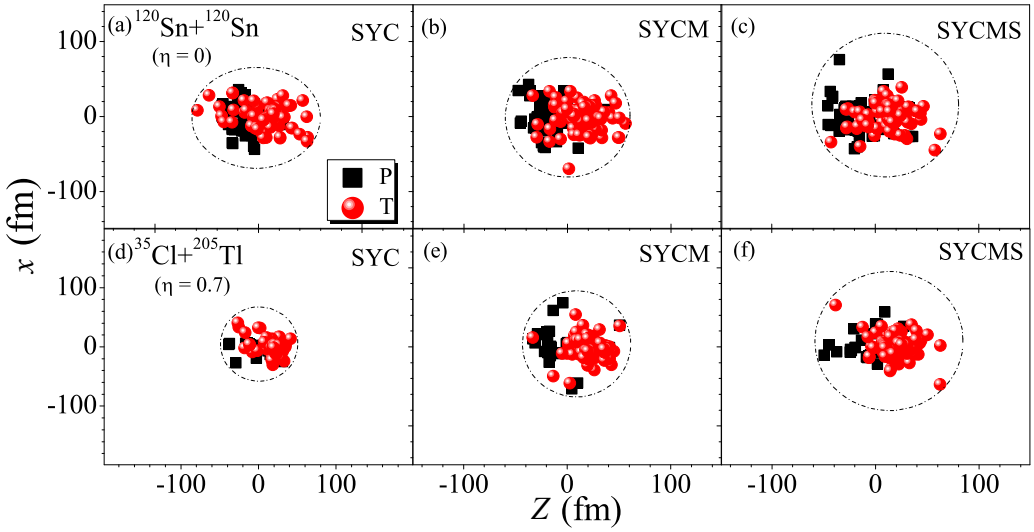

FIG. 1. Phase space of nucleons for ^{120}Sn + ^{120}Sn ($\eta = 0$) [upper panel, (a)–(c)] and ^{35}Cl + ^{205}Tl ($\eta = 0.7$) [lower panel, (d)–(f)] reactions, at $E = 50$ MeV/nucleon and $t = 200$ fm/c for the SYC, SYCM, and SYCMS sets of potentials (shown from left to right).

addition of other parts of the NN potential. The acronym SYC stands for Skyrme + Yukawa + Coulomb potentials, SYCM stands for Skyrme + Yukawa + Coulomb + momentum dependent potentials, and SYCMS stands for Skyrme + Yukawa + Coulomb + momentum dependence + symmetry potentials (as given in Fig. 1).

We begin with the phase space of nucleons of projectile and target nuclei in the X-Z plane, as shown in Fig. 1, for the symmetric as well as the asymmetric reaction of ^{120}Sn + ^{120}Sn [Figs. 1(a)–1(c)] and ^{35}Cl + ^{205}Tl reactions [Figs. 1(d)–1(f)], respectively. Calculations are performed for three different sets of potentials at $E = 50$ MeV/nucleon. One observes that the addition of repulsive MDI and symmetry potential suppresses the high density phase of the reaction. The repulsive behavior of symmetry and MDI potential pushes the matter away from the central dense zone and hence shows the more scattered distribution of projectile and target nucleons [as shown in Figs. 1(b) and 1(c) and Figs. 1(e) and 1(f)]. It is evident that the encircled dotted portion becomes larger with the addition of MDI and symmetry potential. This illustrates the effect of MDI and symmetry potentials on the phase space of nucleons, hence it is interesting to study further how these different potentials affect the production of different fragments in the heavy-ion reaction. It is further explored through the time evolution of density from the initial state (when the nuclear mater is nonequilibrated) to the final state (when the nuclear matter is cold and fragmented). Figure 2 shows the time evolution of mean density in the ^{120}Sn + ^{120}Sn reaction at $E = 50$ MeV/nucleon. The different lines indicate the analysis for different sets of potentials. As the reaction proceeds, the density rises and reaches the maximum at $t = 20$–30 fm/c, when the matter is highly compressed, and finally decreases during the expansion phase. The maximum value of density decreases with the addition of symmetry and MDI potential. This decrease of maximum value may be due to the larger effect of the repulsive nature of MDI and symmetry potential, which in turn pushes the nuclear matter away from the central dense zone and hence prohibits the compression of nuclear matter to a significant level.

Figure 3 shows the charge distribution of fragments for central collisions of (a) ^{120}Sn + ^{120}Sn ($\eta = 0$), (b)^{82}Kr + ^{158}Gd ($\eta = 0.3$), (c)^{56}Fe + ^{184}W ($\eta = 0.5$), and (d)^{35}Cl + ^{205}Tl ($\eta = 0.7$) at $E = 50$ MeV/nucleon. The addition of MDI results in a repulsive interaction between the colliding nucleons, due to which heavy fragments cannot be produced. The difference in charge distribution due to different sets of potentials explores the importance of momentum dependent and symmetry

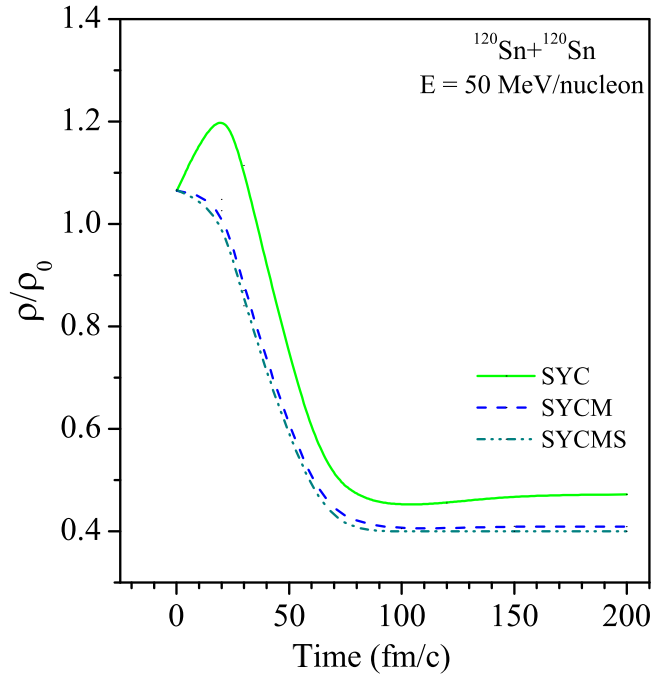

FIG. 2. Time evolution of mean density for the ^{120}Sn + ^{120}Sn reaction at $E = 50$ MeV/nucleon for different sets of potentials.

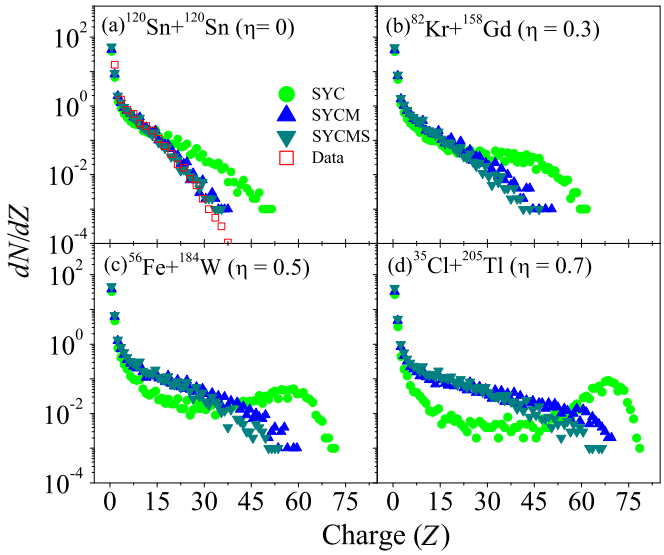

FIG. 3. Charge distribution of fragments for the central collision of the reactions (a) ^{120}Sn + ^{120}Sn ($\eta = 0$), (b) ^{82}Kr + ^{158}Gd ($\eta = 0.3$), (c) ^{56}Fe + ^{184}W ($\eta = 0.5$), and (d) ^{35}Cl + ^{205}Tl ($\eta = 0.7$) at $E = 50$ MeV/nucleon for different sets of potentials and comparison with experimental data [50] for the $\eta = 0$ reaction.

potentials in the reaction dynamics. It is important to note here that the complete set of NN potential (SYCMS) leads to enhanced emission of clusters with low charge (Z) in comparison to the SYC and SYCM sets of potentials. Moreover, the comparison between the calculations and the experimental data [50] for the symmetric reaction ($\eta = 0$) reaction reveals that the momentum dependent potential and symmetry potential are indispensable to explain the charge distribution.

Figure 4 shows the variation of the multiplicity of LCPs in the participant rapidity region [Figs. 1(a)–1(d)] and quasiparticipant rapidity region [Figs. 1(e)–1(h)] with energies for different mass asymmetric reactions. It further explores the contribution of different parts of the NN interaction potential towards fragment production in different rapidity domains. The complete range of rapidity distribution is divided into two different regions, namely, the PR and QPR regions. First, in both PR and QPR regions, the multiplicity of LCPs decreases with the increase in mass asymmetry (η) because of decrease in the participant zone. Second, at low bombarding energies, due to less availability of phase space, NN collisions are less probable. At higher bombarding energies, the violence of reaction increases due to increase in the number of NN collisions, thus leading to an enhanced multiplicity of LCPs.

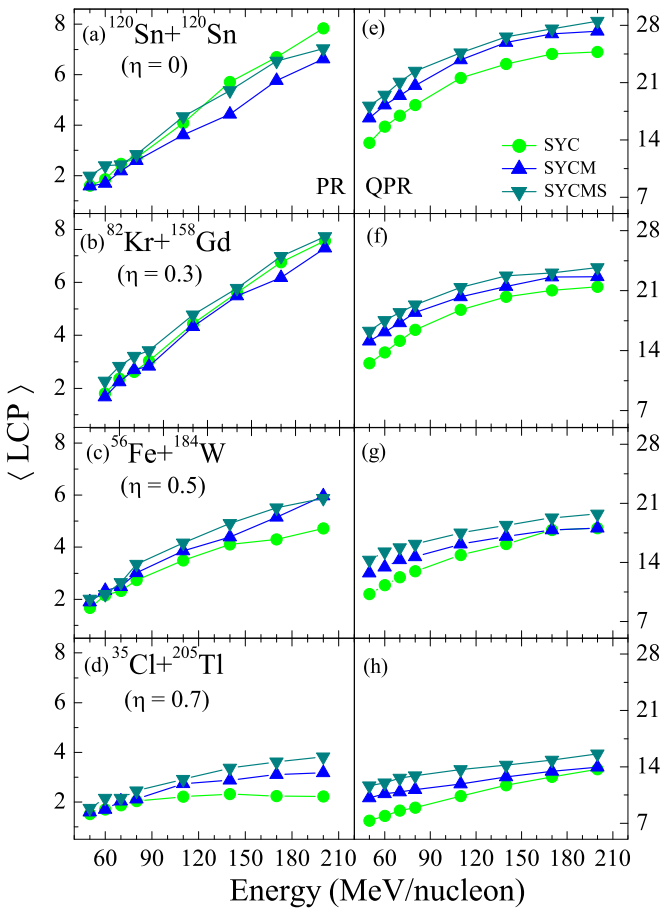

FIG. 4. Variation of the multiplicity of light charged particles in the participant region (left panel) and quasiparticipant region (right panel) with energies for different η.

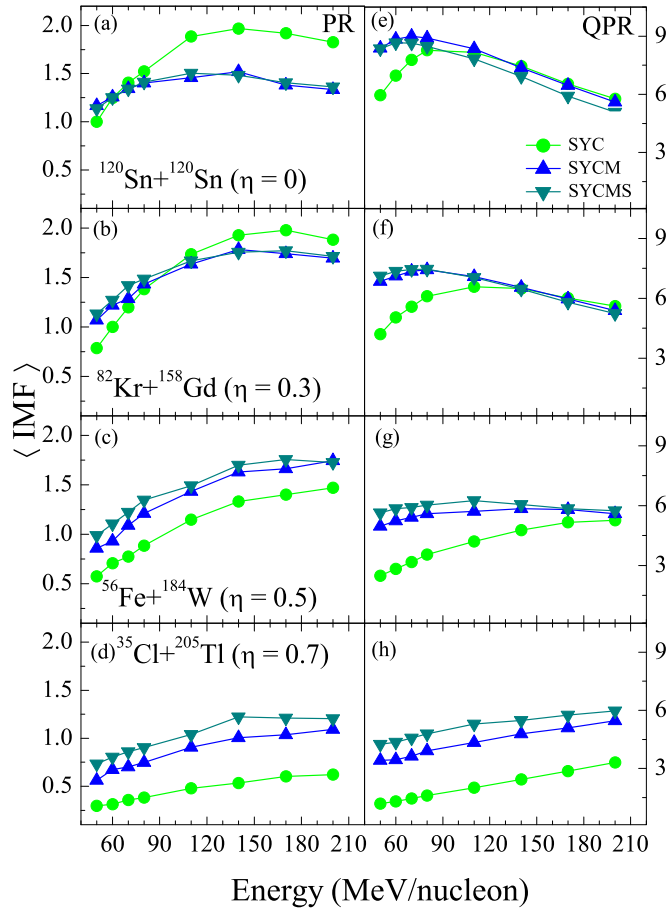

FIG. 5. Variation of the multiplicity of intermediate-mass fragments in the participant region (left panel) and quasiparticipant region (right panel) with energies for different η.

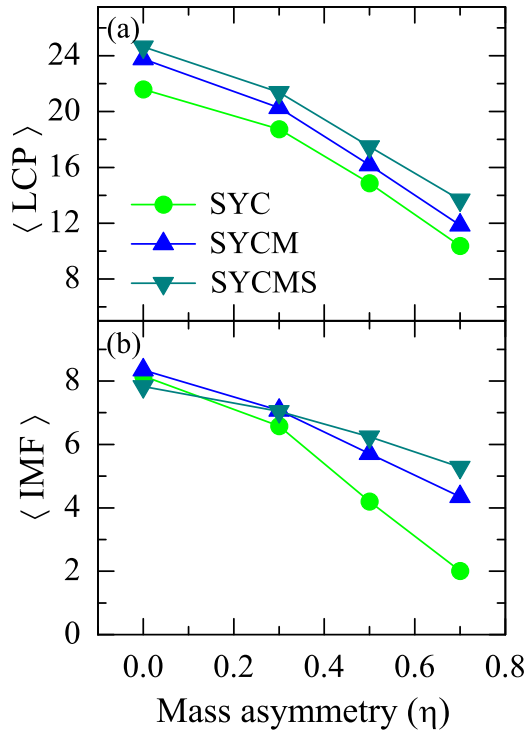

FIG. 6. Variation of (a) LCP and (b) IMF multiplicity in the quasiparticipant region with η at $E = 110$ MeV/nucleon.

Third, for a particular η, the multiplicity is less for the SYC set of potentials. The gradual addition of different potentials imparts further repulsion to the colliding projectile and target combination. The inclusion of MDI leads to increase in the multiplicity of LCPs. Hence the momentum dependent interactions play a dominant role while the symmetry potential has a minor influence on fragment production. It is relevant to mention here that the minor role of the symmetry potential arises due to increase in neutron content of colliding partners.

Figure 5 is similar to Fig. 4 except that it is plotted for IMFs. In both PR and QPR region, the multiplicity of the IMFs decreases with the increase in mass asymmetry which is due to the breaking of heavy-mass fragments into a greater number of free nucleons and LCPs. In the QPR region, the IMFs shows the well-known trend of rise and fall with energy. The peak shifts towards the right with an increase in mass asymmetry (η) of the reaction because more energy is needed to break the heavier fragments due to less compression in mass asymmetric reactions. For $\eta = 0.7$, the multiplicity of the IMFs shows only the rise. It is worth mentioning here that the symmetric reactions ($\eta = 0$) lead to enhanced emission of LCPs and IMFs as compared to asymmetric reactions. This is because of the violent NN collisions between the nucleons of symmetric nuclei. To clearly bring about the importance of MDI and symmetry potential, the mass asymmetry dependence of the multiplicity of LCPs and IMFs in the QPR region at $E = 110$ MeV/nucleon is shown in Fig. 6. Due to the violence of collision at this energy, different sets of potentials behave in a similar manner at $\eta = 0$ (symmetric reaction) and the maximum number of LCPs and IMFs is observed for the symmetric reaction. With an increase in mass asymmetry of the reaction, for the SYC set of potential, a fewer number of fragments are produced. The gradual addition of MDI and symmetry potentials leads to increase in the multiplicity of LCPs and IMFs and hence shows their significance in fragment production.

IV. SUMMARY

The role of different parts of the NN interaction potential on the production of LCPs and IMFs within different rapidity domains has been studied using the IQMD model. The analysis has been done by keeping the total mass of the system constant ($A_{\text{total}} = 240$ units) and by varying the mass asymmetry of colliding nuclei from 0 to 0.7. We find that the multiplicity of different fragments changes with the gradual addition of different parts of the NN interaction potential. The comparison between calculations and experimental data for ^{120}Sn + ^{120}Sn reaction reveals that both MDI and symmetry potential are necessary to explain the charge distribution. The MDI plays a dominant role and the symmetry potential has minor influence on fragment production yet both together lead to increase in the multiplicity of LCPs and IMFs and hence are indispensable to study fragment production.

ACKNOWLEDGMENTS

V.K. acknowledges support by the Department of Science and Technology, New Delhi under the SERC Fast Track Scheme, Grant No. SR/FTP/PS-020/2012. We are also thankful to Prof. Rajeev K. Puri for giving access to his various computer programs for the current work.

[1] C. L. Jiang, K. E. Rehm, B. B. Back, H. Esbensen, R. V. F. Janssens, A. M. Stefanini, and G. Montagnoli, Phys. Rev. C **89**, 051603(R) (2014).
[2] B. B. Back, H. Esbensen, C. L. Jiang, and K. E. Rehm, Rev. Mod. Phys. **86**, 317 (2014).
[3] R. K. Puri and R. K. Gupta, Phys. Rev. C **51**, 1568 (1995).
[4] G. G. Adamian, N. V. Antonenko, and W. Scheid, Phys. Rev. C **69**, 044601 (2004); V. I. Zagrebaev, A. V. Karpov, and W. Greiner, *ibid.* **85**, 014608 (2012).
[5] V. Kaur and S. Kumar, J. Phys. G **39**, 085114 (2012).
[6] S. Kaur and R. K. Puri, Phys. Rev. C **87**, 014620 (2013).
[7] A. D. Sood, R. K. Puri, and J. Aichelin, Phys. Lett. B **594**, 260 (2004).
[8] S. Gautam, A. D. Sood, R. K. Puri, and J. Aichelin, Phys. Rev. C **83**, 034606 (2011).
[9] V. Kaur, S. Kumar, and R. K. Puri, Phys. Lett. B **697**, 512 (2011).
[10] V. Kaur, S. Kumar, and R. K. Puri, Nucl. Phys. A **861**, 37 (2011).
[11] R. K. Puri, R. Arora, and R. K. Gupta, Phys. Rev. C **60**, 054619 (1999).

[12] V. Zanganeh, N. Wang, and O. N. Ghodsi, Phys. Rev. C **85**, 034601 (2012).
[13] D. T. Khoa, N. Ohtsuka, M. A. Matin *et al.*, Nucl. Phys. A **548**, 102 (1992).
[14] R. K. Puri, P. Chattopadhyay, and R. K. Gupta, Phys. Rev. C **43**, 315 (1991).
[15] R. K. Puri and R. K. Gupta, Phys. Rev. C **45**, 1837 (1992).
[16] J. Jaenicke, J. Aichelin, N. Ohtsuka, R. Linden *et al.*, Nucl. Phys. A **536**, 201 (1992).
[17] S. A. Bass, C. Hartnack, H. Stocker, and W. Greiner, Phys. Rev. Lett. **71**, 1144 (1993).
[18] S. R. Souza, B. V. Carlson, R. Donangelo, W. G. Lynch, A. W. Steiner, and M. B. Tsang, Phys. Rev. C **79**, 054602 (2009).
[19] M. D'Agostino, G. J. Kunde, P. M. Milazzo, J. D. Diniu, M. Bruno, N. Colonna, M. L. Fiandri, C. K. Gelbke, T. Glasmacher, F. Gramegna *et al.*, Phys. Rev. Lett. **75**, 4373 (1995).
[20] J. Y. Liu, W. J. Guo, Y. Z. Xing, X. G. Li, and Y. Y. Gao, Phys. Rev. C **70**, 034610 (2004).
[21] A. Ergun, H. Imal, N. Buyukcizmeci, R. Ogul, and A. S. Botvina, Phys. Rev. C **92**, 014610 (2015).
[22] S. Goyal, Phys. Rev. C **83**, 047604 (2011).
[23] C. Gale, G. F. Bertsch, and S. Das Gupta, Phys. Rev. C **35**, 1666 (1987); C. Gale, G. M. Welke, M. Prakash, S. J. Lee, and S. Das Gupta, *ibid.* **41**, 1545 (1990).
[24] G. Peilert, H. Stöcker, W. Greiner, A. Rosenhauer, A. Bohnet, and J. Aichelin, Phys. Rev. C **39**, 1402 (1989); M. Berenguer, C. Hartnack, G. Peilert, H. Stöcker *et al.*, J. Phys. G **18**, 655 (1992).
[25] J. Aichelin, A. Rosenhauer, G. Peilert, H. Stöcker, and W. Greiner, Phys. Rev. Lett. **58**, 1926 (1987).
[26] S. Kumar and R. K. Puri, Phys. Rev. C **60**, 054607 (1999); J. Singh, S. Kumar, and R. K. Puri, *ibid.* **63**, 054603 (2001); Y. K. Vermani, S. Goyal, and R. K. Puri, *ibid.* **79**, 064613 (2009).
[27] H. Zhou, Z. Li, and Y. Zhuo, Phys. Rev. C **50**, R2664 (1994).
[28] B. A. Li, L. W. Chen, and C. M. Ko, Phys. Rep. **464**, 113 (2008).
[29] W. D. Myers and W. D. Swaiatecki, Nucl. Phys. **81**, 1 (1996).
[30] S. Gautam, R. Kumari, and R. K. Puri, Phys. Rev. C **86**, 034607 (2012).
[31] M. B. Tsang, T. X. Liu, L. Shi, P. Danielewicz *et al.*, Phys. Rev. Lett. **92**, 062701 (2004).
[32] M. A. Famiano, T. Liu, W. G. Lynch, M. Mocko *et al.*, Phys. Rev. Lett. **97**, 052701 (2006).
[33] M. B. Tsang, Y. Zhang, P. Danielewicz, M. Famiano, Z. Li, W. G. Lynch, and A. W. Steiner, Phys. Rev. Lett. **102**, 122701 (2009).
[34] L. W. Chen, C. M. Ko, and B. A. Li, Phys. Rev. Lett. **94**, 032701 (2005).
[35] L. W. Chen, C. M. Ko, and B. A. Li, Phys. Rev. C **69**, 054606 (2004).
[36] J. Xu, L. W. Chen, B. A. Li, and H. R. Ma, Phys. Rev. C **77**, 014302 (2008).
[37] M. Kaur, V. Kaur, and S. Kumar, Phys. Rev. C **88**, 054620 (2013); V. Kaur, M. Kaur, and S. Kumar, Nucl. Data Sheets **118**, 333 (2014).
[38] W. Reisdorf, Nucl. Phys. A **630**, 15 (1998).
[39] Y. Zhang, C. S. Zhou, J. X. Chen, N. Wang *et al.*, Sci. China: Phys., Mech. Astron. **58**, 112002 (2015).
[40] M. B. Tsang, C. Williams, M. J. Huang, W. G. Lynch *et al.*, Phys. Rev. C **55**, R557 (1997).
[41] S. Kumar, S. Kumar, and R. K. Puri, Phys. Rev. C **78**, 064602 (2008).
[42] A. Schuttauf, W. D. Kunze, A. Wörner, M. B. Blaich *et al.*, Nucl. Phys. A **607**, 457 (1996).
[43] C. Hartnack, R. K. Puri, J. Aichelin, J. Konopka *et al.*, Eur. Phys. J. A **1**, 151 (1998).
[44] C. Hartnack, H. Oeschler, Y. Leifels, E. L. Bratkovskaya *et al.*, Phys. Rep. **510**, 119 (2012).
[45] J. Aichelin, Phys. Rep. **202**, 233 (1991).
[46] E. Lehmann, R. K. Puri, A. Faessler, G. Batko, and S. W. Huang, Phys. Rev. C **51**, 2113 (1995).
[47] E. Lehmann, R. K. Puri, A. Faessler, T. Maruyama *et al.*, Prog. Part. Nucl. Phys. **30**, 219 (1993).
[48] S. Gautam, J. Phys. G **37**, 085102 (2010).
[49] S. Gautam, A. D. Sood, R. K. Puri, and J. Aichelin, Phys. Rev. C **83**, 014603 (2011).
[50] S. Hudan, A. Chbihi, J. D. Frankland, A. Mignon *et al.*, Phys. Rev. C **67**, 064613 (2003).